IOP Publishing | Astro Ltd Laser Physics
Laser Phys. **26** (2016) 084005 (17pp) doi:10.1088/1054-660X/26/8/084005

Diamond device architectures for UV laser monitoring

S Salvatori[1], M Girolami[2], P Oliva[1,3], G Conte[2,4], A Bolshakov[5,6], V Ralchenko[5,6] and V Konov[5,6]

[1] University Niccolò Cusano, Via Don Carlo Gnocchi 3—00166 Rome, Italy
[2] Institute for Structure of Matter, CNR-ISM, Via Salaria km 29,300, Montelibretti, Italy
[3] Mediterranean Institute of Fundamental Physics 'MIFP' - Via Appia Nuova 31, 00040 Marino (Rome), Italy
[4] Department of Sciences, University Roma Tre, Via Vasca Navale 84—00148 Rome, Italy
[5] A.M. Prokorhov General Physics Institute, RAS, Vavilova 38—119991 Moscow, Russia
[6] National Research Nuclear University 'MEPhI', Kashirskoye shosse 31—115409 Moscow, Russia

E-mail: gconte@fis.uniroma3.it

Received 11 May 2016
Accepted for publication 22 May 2016
Published 30 June 2016

Abstract

The paper reviews the status of diamond detectors for UV laser monitoring and imaging. Single pixel detectors, position sensitive architectures, optically activated switches and sensor arrays for beam positioning and imaging are analyzed. The performances of natural diamond and synthetic diamond produced by chemical vapor deposition are compared to evaluate the suitability of such an outstanding material for the described applications.

Keywords: excimer lasers, pixel array detector, single pixel detector, diamond

(Some figures may appear in colour only in the online journal)

1. Introduction

Diamond is a material with a very compact lattice (1.76×10^{23} at cm^{-3}) and the highest covalent bond strength (347 $kJ \cdot mol^{-1}$). Energies as high as 45 eV have been demonstrated to be necessary in order to displace a single atom from such a compact structure [1]. The very high cohesive energy in crystalline diamond is responsible for the highest Young modulus (1100 GPa) and thermal conductivity ($22\,W \cdot cm^{-1} \cdot K^{-1}$) we find in comparison to any other solid, together with a small thermal expansion coefficient (0.8×10^{-6} K^{-1} at 300 K). These properties and the outstanding hardness value are reflected in superior electronic properties of the material [2], in the form of a large breakdown electric field that makes the diamond a promising choice for high voltage and high-power applications, qualifying it as an excellent dielectric at room temperature or a wide bandgap semiconductor in high temperature conditions, too. Moreover, charge carrier mobility as high as 4500 and 3800 $cm^2 \cdot V^{-1} \cdot s^{-1}$, for electrons and holes respectively, have been reported by Isberg *et al* [3] together with a very high saturation drift velocity ($\sim 2 \times 10^7$ $cm \cdot s^{-1}$). Using time-of-flight measurements, charge carrier lifetimes as high as 0.321 μs for electrons and 0.983 μs for holes have been reported in synthetic diamond samples [4] deposited by microwave plasma assisted CVD techniques.

Gracio *et al* [2], reported that the most important diamond parameters remain the same also for polycrystalline diamond, especially for larger grained films. As depicted by Collins [5], polycrystalline-CVD diamond can be considered an elective material for the realization of electronic devices and sensors. Indeed, thanks to the unique characteristics mentioned above, diamond has been considered eligible for the fabrication of UV photoconductive switches and devices [6–9]. Moreover, it seems suitable for detection and imaging of UV radiation in harsh environments up to the x-ray region. The very high thermal conductivity, together with the mechanical and electronic features, ensure good power dissipation, absence of thermal runaway, high charge collection efficiency, high signal sensitivity, fast transient response, low noise and radiation hardness. In addition, such an unusual material had extensive exploitation for passive and active electronic devices and photodetectors able to monitor fast pulsed sources like UV excimer lasers and synchrotron radiation beams in the UV-XUV region. Nowadays, the lack of commercial wide area single crystal diamond substrates is again limiting the development of innovative detectors even if some interesting ideas

for convenient substrates have been demonstrated [10, 11, 12] together with the implementation of detectors based on a mosaic of small high quality plates [13] in order to cover large area requirements. A status review of diamond detectors for UV laser monitoring and beam imaging is presented in the following sections. Section 2 reports the most important spectroscopic characteristics of single crystal and polycrystalline diamond as well as the features expected for fast high voltage UV switching; section 3 depicts the requirements for single-pixel devices in pulsed laser detection; section 4 discusses optically activated phototransistors; section 5 is about the position-sensitive detectors and, finally, section 6 analyzes the devices with a pixel architecture implemented for beam imaging.

2. Diamond: a high energy photoconductive material

Among wide band gap semiconductors, diamond shows photoconductive characteristics, mainly dependent on its bulk morphology (e.g. monocrystalline natural stone, epitaxial crystal, poly- or nano-crystalline film). Moreover, mosaic effects, average grain dimension, texturing, boundary defect passivation and local stress produced by mechanical treatments carried out for plates-cutting or surface roughness reduction, strongly influence its optoelectronic behavior. The static performance of a photoconductive material can be characterized by the dark current $I_d = \sigma_d AF$ and the photocurrent $I_{ph} = (\sigma_L - \sigma_d)AF$, where σ_d is the dark conductivity, σ_L the conductivity under illumination, A the electrode area and F the applied electric field strength. From the photocurrent signal measurement, two widely used parameters can be derived:

(i) the photoconductive gain, G_{ph}, which is a quantity independent of the semiconductor optical properties [14]:

$$G_{ph} = I_{ph}/qN_0\eta_{abs} \tag{1}$$

where q is the electron charge, N_0 the number of incident photons per unit time and η_{abs} the optical absorption efficiency;

(ii) the responsivity, R_{ph}, which contains information on the material spectral characteristics:

$$R_{ph} = I_{ph}/qN_0h\nu \tag{2}$$

$h\nu$ being the photon energy expressed in eV.

According to a simple photogeneration and collection model [15], the total photocurrent can be written as:

$$I_{ph} = qN_0\eta_{abs}\mu\tau F/d \tag{3}$$

where $\mu\tau$ is the mobility-lifetime product of photogenerated carriers and d the inter-electrode spacing.

Then the photocurrent gain equals the ratio between the drift collection distance $L = \mu\tau F$ and the electrode spacing:

$$G_{ph} = \mu\tau F/d \tag{4}$$

therefore giving values much higher than unity, even at low fields, for sufficiently narrow electrode gaps. Within the theoretical structure, the absorption efficiency is described by the relationship:

$$\eta_{abs} = (1 - R)\,[1 - e^{-\alpha t}] \tag{5}$$

where R is the optical reflectivity, α the absorption coefficient and t is the active device thickness. As a consequence, the spectral responsivity around the bandgap can be simply calculated by substitution of (3) and (5) into (2):

$$R_{ph} = (1 - R)[\alpha t/h\nu]G_{ph}. \tag{6}$$

In deriving (6), $\alpha t \ll 1$ was assumed since typical values of the diamond absorption coefficient around the bandgap are $\sim 100\,cm^{-1}$ [16] and the active thickness of the investigated films (e.g. the penetration depth for the planar contact configuration) was about 10 μm. At room temperature, intrinsic diamond starts to exhibit a substantial photoconductive signal for photon energies greater than 5.25 eV ($\lambda < 236$ nm), whereas it has a negligible response to visible and near-ultraviolet radiation as shown in figure 1. Within the spectral range extending from 2.5 to 4.5 eV, the signal reflects the joint density of defective states inside the bandgap [6, 17]. The exponential increase near the bandgap energy is due to electronic transitions between the Urbach tails, due to the angle and length variations of nearest neighborhood carbon bonds, and the extended states. At photon energies higher than the diamond bandgap, the penetration depth is reduced to a fraction of microns. In such a case, photon absorption and charge carrier generation take

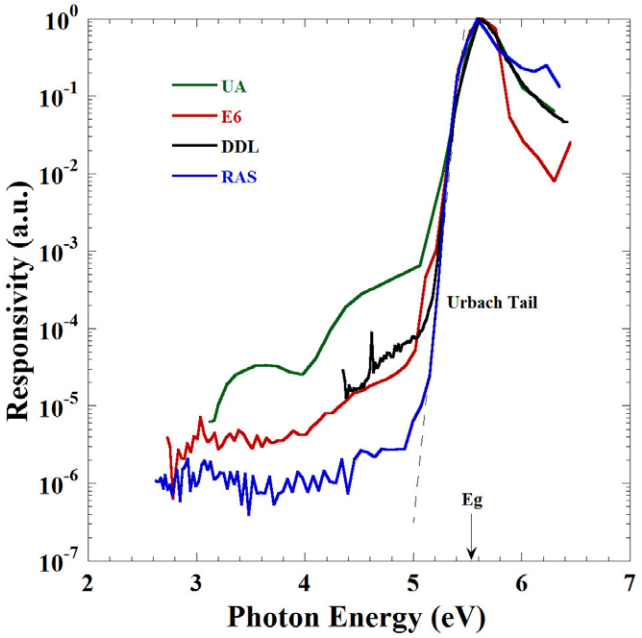

Figure 1. Single crystal diamond responsivity, normalized to maximum, versus photon energy of polished plates, 0.5 mm thick, by different source: UA, Ural Almazinvest, Type II Natural Diamond; E6, Element Six, epi-CVD; DDL, Diamond Detector Ltd, epi-CVD; RAS, General Physics Institute, Russian Academy of Sciences, epi-CVD. For all the samples, silver grids with interdigitated fingers 200 nm thick and 40 μm apart have been used as planar contacts. Monochromatic light was chopped at 13 Hz; photocurrent signal was measured as the voltage at the output of an I–V converter, waiting for the time needed to reach the necessary amplitude regime value.

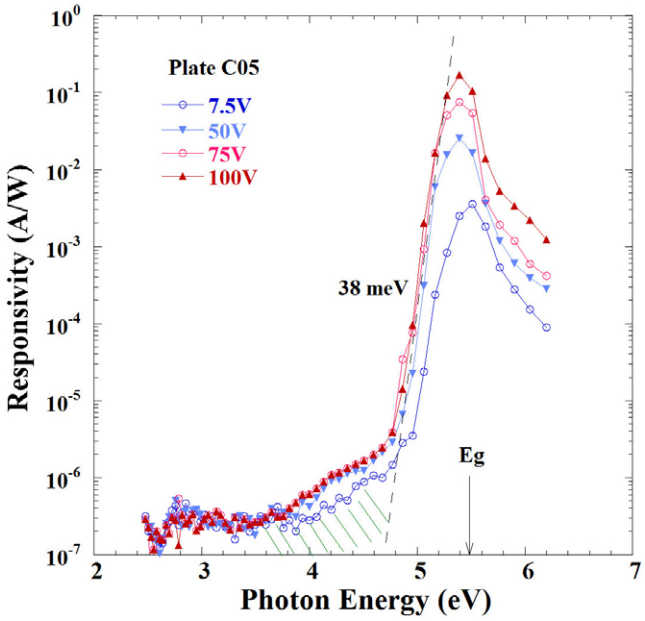

Figure 2. Responsivity dependence on the photon energy, for different applied voltages, of a single crystal diamond plate grown by plasma assisted CVD epitaxy, detector grade quality, by DDL (Diamond Detectors Ltd, UK). Silver was used as the metal for the contacts having an interdigitating configuration with fingers 40 μm apart. The green hatched area depicts the transition between defect and extended states.

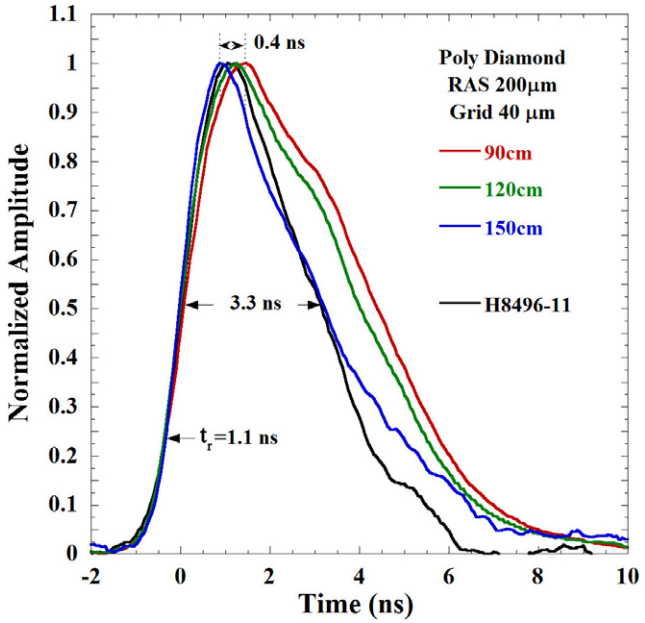

Figure 3. The temporal pulse shape of ArF Neweks PSX-100 excimer laser (193 nm, 10 Hz, 4.5 mJ per pulse) as measured by Hamamatsu H8946-11 phototube and a polycrystalline diamond plate, 0.2 mm thick, by GPI RAS. A silica lens, $f = 10$ cm, was inserted at the laser output to obtain light dispersion in order to allow measurements as a function of photon density (just increasing lens-sample distance). An interdigitated Cr/Au grid, with fingers 40 μm apart, was used as the sample contact to perform measurements. 30 volts were applied to the diamond film through a Picosecond 5575A bias tee whereas the photocurrent signal was recorded as the voltage across the 50 Ω input impedance of a LeCroy Wavepro 960 digital sampling oscilloscope.

place mainly at the film surface where defects, mainly due to the performed mechanical polishing, strongly affect the photoresponse of sensors. Even though average surface roughness as low as 2–4 nm has been obtained with fine polishing treatments, the active electronic states could recombine the photogenerated charge carriers leading to a responsivity signal loss. This signal is strongly dependent on the device configuration [18, 19] and can be partially recovered by increasing the applied electric field as illustrated in figure 2. The responsivity around the bandgap energy improves by about two orders of magnitude increasing the applied voltage from 7.5 V (1.8×10^3 V · cm^{-1}) to 100 V (2.5×10^4 V · cm^{-1}), whereas the surface recombination effect still induces a signal decrease for photon energies greater than 5.5 eV. The photoconductive selectivity, also called 'solar blindness', e.g. the ratio between over-gap and below-gap signals, is in excess of 10^6 for this homo-epitaxial diamond sample: generally, the selectivity is an indication of the material quality and the samples are classified from 'sensor grade' to 'electronic grade' films. High selectivity was also demonstrated for polycrystalline diamond. McKeag *et al* [20] obtained values in excess of 10^6 after heating a small grained CVD diamond sample at 700 °C for 1 h in methane, followed by heating at 400 °C for 1 h in air. This treatment was able to reduce the sub-bandgap photoconductivity, increasing the ratio between the over-gap and below-gap responses. Such a high selectivity value leads to the suitability of diamond for daylight UV sensor applications.

Interesting performance can also be found when intense UV pulsed-laser light illuminates the diamond surface as that depicted in figure 3 acquired under a pulsed excimer laser source. Here the photoresponse of a detector fabricated using polycrystalline CVD diamond by GPI RAS is compared to that of a Hamamatsu phototube irradiated by the same ArF 193 nm laser. The asymmetric peak shape, also returned by the phototube, reflects the typical temporal excitation and fall of electrons inside the excimer gas mixture. A silica lens, inserted in the laser output, was used for light beam dispersion in order to decrease the impinging photons, intensity on the diamond detector by increasing the sensor-lens distance. At the lower beam intensities (e.g. 150 cm from the lens focus), the peak shapes acquired for the diamond sample and the phototube can be considered almost the same taking into account the different electronic noise coupled to the two detectors. The pulse rise time is 1.1 ns with a FWHM of 3.3 ns. Decreasing the sensor distance from the lens focus, the signal dependence on the beam intensity shows two different regimes following a power-law for the signal that behaves like kI^β [21, 22], I being the integral beam intensity and k a proportionality constant; $\beta = 1$ leads to a linear response observed at lower intensities while $\beta = 0.5$ indicates a sub-linear trend at higher ones, as reported in figure 4. Further details on such a behavior will be indicated in the following section 3.

All the above cited characteristics, together with the high thermal conductivity and lower thermal expansion coefficient, make the diamond a superb window material and a suitable photoconductive medium for fast high-voltage and high-power optical switching. In its simplest form, such a

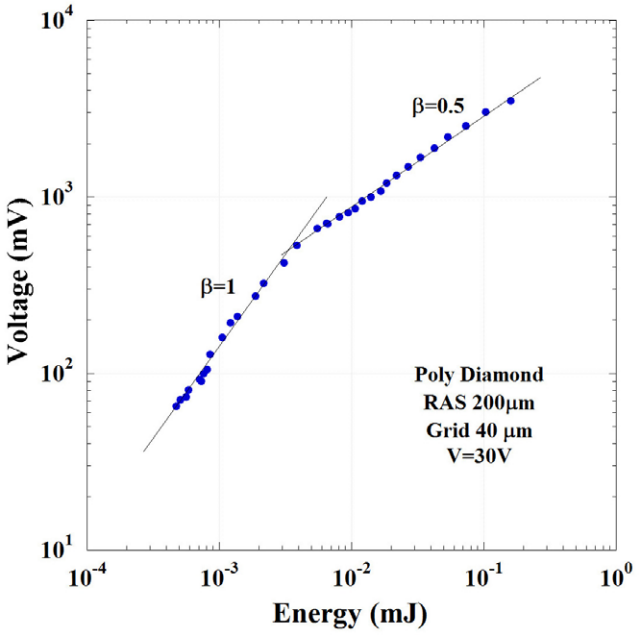

Figure 4. Polycrystalline CVD diamond peak amplitude versus the ArF excimer laser energy (measured with a Molectron J3-05 power meter). The laser was a Neweks PSX-100, 193 nm, 10 Hz, 4.5 mJ per pulse. A silica lens, $f = 10$ cm, was inserted at the laser output in order to perform the characterization as a function of the impinging photon intensity (see text). The measurement used a front interdigitated Cr/Au grid with fingers 40 μm apart and 30 V as applied bias.

solid-state device consists of a piece of intrinsic diamond with two metal contacts whose gap defines the sensing area. A photoconductive switch can be instantly closed by the creation of charge carriers within the gap due to a short pulse illumination, in such a way decreasing the bulk resistance from tenths of TΩ to tens of Ω. Conduction stops as soon as incident irradiation falls down, being the electron–hole pair recombination time just around 50 ps. The switching speed, depending on the rise time τ_R and the fall time τ_F, is one of the most important parameters of such devices. While τ_F mainly depends on carrier lifetime, τ_R relates to the propagation time over the interelectrode gap distance d [23]:

$$\tau_R = 1.5\sqrt{\varepsilon}\, d/c \tag{7}$$

ε being the dielectric constant and c the speed of light in vacuum. In order to reduce the rise time, a low dielectric constant material has to be chosen and the interelectrode gap should be lowered. Compared with other wide gap semiconductors used for this application, diamond has a smaller dielectric constant together with a higher electrical breakdown voltage, assuring high voltage handling, while showing worse carriers lifetime. This application, not yet completely exploited, was studied in the 1980s by Ho *et al* [24] using type IIa natural diamond as a photoconductor excited by picosecond laser pulses of a frequency-tripled Nd:YAG laser. Bharadwaj *et al* [25] reported results on the characteristics of a high performance sub-nanosecond optoelectronic switch based on the photoconductivity of natural type IIa diamonds. Successively, Panchhi *et al* [26] have studied the temporal response of the photoconductivity for different types of natural diamonds using picosecond 1.06, 0.53, 0.35 and 0.266 μm pulses of a Nd:YAG laser. The measured characteristic time constant was remarkably close to the 150 ps value. All diamonds showed a linear response to the light intensity up to approximately 100 MW · cm^{-2}. Garnov *et al* [27] reported a comparison of type IIa and CVD diamond photogenerated carrier properties using a lab-made picosecond Nd:YAG laser with high stable second, third and fourth harmonics used as a source of excitation light. To record the photocurrent signal, samples were positioned between flat electrodes with applied pulsed electric field up to 4 kV · cm^{-1} synchronized with exciting laser pulses. Feng *et al* [28] succeeded with electric fields as high as 1 MV · cm^{-1} again using a type IIa natural diamond obtaining on-resistances as low as 30 Ω on a 200 μm thick plate. In this case, the gap between the metal contacts was irradiated with a KrF excimer laser ($\lambda = 248$ nm, 2 mJ per pulse 10–15 ns of pulse duration) absorbed by the presence of electronic states within the diamond gap. Experiments demonstrated reliable operation and switching performances with high repetition rate, at least up to 18 MHz. Aikawa *et al* [29] tested the suitability of polycrystalline CVD diamond for this application. The authors described performances up to 2×10^6 V · cm^{-1} by using a 248 nm KrF laser shining light on the device.

Although diamond has been depicted as the most 'radiation hard' material, it has also been shown that damage can be produced at laser fluence levels considerably below that required for material graphitization [30] or cutting. The optical breakdown threshold, however, has not exactly been defined because of its dependence on the material's morphology, surface contamination, and beam parameters like the laser pulse duration, repetition rate, etc. The first study of long term pulse exposure and fluence level effect on the performance of CVD diamond photodetectors was performed by Whitfield *et al* [31] using a 193 nm excimer laser over-gap radiation. The results showed that a diamond film, exposed to 10^6 laser pulses in air with energies greater than 10 mJ · cm^{-2}, gets visibly damaged appearing whitish and opaque. In the same paper, experiments with F_2 laser at 157 nm were carried out to evaluate the effect of direct absorption transitions: indeed, while at 193 nm the electron excitation involves a phonon-assisted process, at 157 nm the transition is direct and could activate different degradation processes. The devices exhibited a good response up to a fluence of 1.4 mJ · cm^{-2} and appeared to be capable of following the temporal behavior of the laser pulse. However, during these tests, the devices were irradiated by a number of pulses between 10^4 and 10^5 with no obvious degradation in characteristics. Nevertheless, photoconductive switches have been developed with CVD diamond films to generate high-power terahertz radiation [32] from an antenna array. In an experiment with ultra-short pulses of KrF laser light, an emission density of 0.1 μJ · cm^{-2} at 10^5 V · cm^{-1} was achieved. Another neat application of photoconductive switches consisted in the control of diamond mirrors in the microwave region. The conductivity of a diamond window was modulated within the in-depth penetration of a UV laser by photogenerated charge carriers, thereby altering

its reflectivity to microwaves. The highest observed reflectivity for 11.424 GHz microwaves was 38% and this percentage was achieved by illuminating the diamond window with 10 ns, 160 mJ pulses at 266 nm by a Nd:YAG laser [33]. Effective diamond RF switches for the X-band application require a laser pulse at least of 300 ns duration, which was not available at that time. The complete exploitation of epitaxial and high quality polycrystalline diamond plates for UV optically activated arrays of switches does not rely on the bulk thickness but only on plate lateral dimensions. The in-phase commutation of many switches is an interesting foreseen application that can find in the epitaxial CVD diamond the material of choice.

3. Diamond based light-sensors for UV laser monitoring

Excimer lasers represent a fundamental tool in several application fields: from the semiconductor VLSI and MEMS industry [34] to the exploitation in stimulating chemical processes, as well as laser-cutting from eye surgery to dermatological treatments [35]. In such a context, wide bandgap solar-blind radiation-hard materials appear very appealing for the realization of suitable detectors, able to ensure a real-time monitoring of the illumination intensity and homogeneity of the laser beam. In this field, as mentioned in section 1, diamond represents a good choice for the development of performing, fast and radiation-hard UV detectors [18, 21, 36, 37] due to its wide bandgap, assuring transparency to VIS-IR radiations (see figure 1) and reducing dark current also for photoconductive devices, with no need for antireflection coatings or wavelength converters. Moreover, its high mobility and saturation velocity of charge carriers ensure a fast photoresponse (as illustrated in figure 3), allowing real-time diagnostics of laser pulses. Finally, the high cohesive energy of carbon atom in diamond specimens and the highest thermal conductivity of the deposits allow a strong reduction in radiation damage, making the employment of attenuators not necessary in the case of high-power source analysis such as excimer lasers or x-ray tubes.

Diamond film quality strongly affects detector photoresponse under intense UV laser irradiation. As stated in section 2, a reduction of the response linearity is expected when the radiation source is a pulsed laser having high peak power. This effect is related to the defect density in undoped samples: for this reason several works investigated the dependency on the pulse energy of the output signal of the sensor based on diamond samples of different quality in order to gain useful information on detector performances under such an illumination condition. Figure 5 shows the experimental results of four different CVD diamond samples, characterized under excimer UV laser irradiation (Neweks PSX 100, $\lambda = 193$ nm, 10 Hz of repetition rate and 4.5 mJ per pulse intensity) [21]. The samples were referred to as D1–D4, where D1 is the film with the highest quality and D4 the one with the poorest. In particular, D1 and D2 have been grown by standard MWCVD technique. For the former, with a grain size of around 200 μm, the best quality has been gained by removing defects both on the growth and

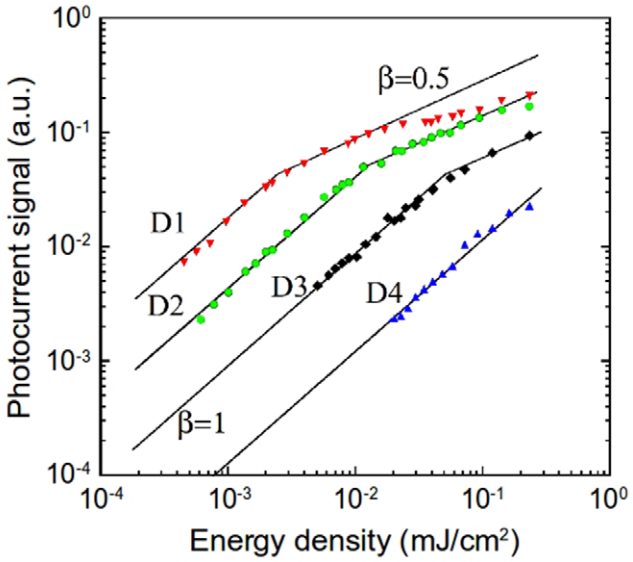

Figure 5. Photocurrent signal as a function of the impinging photon intensity for four diamond samples of different film quality (see text). At low intensities of impinging light a linear dependence of the signal amplitude was observed (exponent $\beta = 1$), whereas at high energy density of light the photoresponse resulted proportional to the squared root of the light intensity ($\beta = 0.5$). The behavior agrees with a transition towards a bimolecular recombination process at very high generation rates. The higher the film quality, the higher the output signal amplitude, and the lower the energy density at which the sub-linear dependency is found.

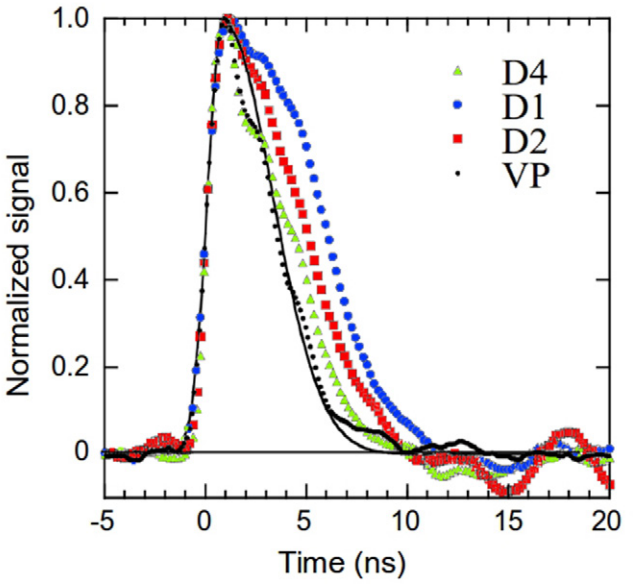

Figure 6. Photocurrent pulse response at low peak laser intensity (<1 μJ) for four different diamond samples of different quality. The higher the quality, the larger the pulse FWHM. VP refers to the response of a fast vacuum phototube (Hamamatsu H8946-11), used as reference. The continuous line represents the best fit of VP data.

substrate-side of the film by mechanical polishing. The latter, 800 μm thick, had a grain size of 100 μm and was mechanically polished only on the growth side. D3 refers to a De Beers sample, 1 mm thick, having a roughness comparable to its grain size around 100 μm. (Such an untreated sample was expected to show lower detection performances in comparison to the other

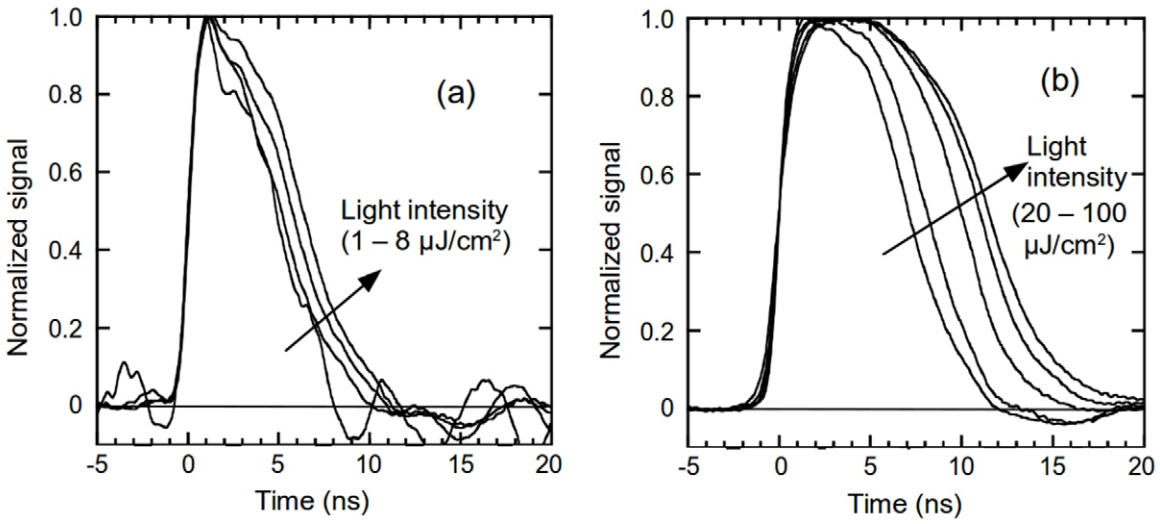

Figure 7. Photocurrent pulse response for (a) low flux (with $\beta = 1$) and (b) high flux (with $\beta = 0.5$) for a good quality diamond film (D2). Light intensity has been changed by less than one order of magnitude, dispersing laser beam by a lens and varying the distance from the lens focus of the irradiated sample.

mentioned films.) Finally, the thin D4 specimen was grown in a HFCVD apparatus exhibiting an average grain size of the order of only 10 μm. After diamond growth, a silver film, of about 1 μm in thickness, was deposited by vacuum thermal evaporation on the diamond growth surface and patterned by standard lithographic technique, in order to obtain an interdigitated multi-finger contact defined as 20 + 20 fingers (60 μm $\times$ 4 mm each) with an inter-electrode distance of 60 μm. As depicted in figure 5 the investigated samples exhibited the expected kI^{β} power law dependence of the photoresponse signal on the pulse energy intensity (see section 2), in good agreement with the theoretical prediction. Indeed, for less defected samples (having a negligible sub-gap photoresponse), as D1 and D2 films, the output signal shows the highest amplitude, together with a linear increase on the pulse energy only at relatively low intensities of the impinging light. A gradual change to a sub-linear dependence is then observed. Hence, for the low density of defect states acting as recombination centers, a pure monomolecular recombination occurs only at low pulse energy, i.e. at a low generation rate during the impinging light pulse. When the pulse energy (and then the generation rate) becomes high enough, the recombination mechanism changes to a bimolecular one [38]. Conversely, samples with a larger defect density, as D3 and D4 specimens, exhibited the lowest photosignal amplitude, but their response linearity is kept until higher pulse energies. Practically, highly defected films, embedding higher density of recombination centers, are able to guarantee a larger range of detector linearity, even if their UV–VIS discrimination ratio will be lower than that observed in high quality samples. Moreover, the normalized photovoltage pulses obtained at lower peak energy (<1 μJ) for different samples are reported in figure 6, where the laser pulse recorded by the vacuum phototube (VP) is also shown for comparison.

For all the investigated samples, the pulse shapes showed a similar decay time, of about 6 ns, for the output signal spanning from the 90% to the 10% of the peak amplitude. According to a higher carrier lifetime in high quality diamond, the FWHM of the output signal pulse was slightly different, increasing from 4 ns, for the highly defected film, to 6 ns, found in the high quality one. Moreover, it is worthwhile to observe that the photovoltage pulse shape was also strongly dependent on the impinging pulse energy, especially for the best quality samples. In figure 7 the results obtained from the D2 sample (grain in the 200–300 μm range, 800 μm thick) are reported. The figure on the left refers to the low light intensity regime, whereas that shown on the right depicts sample photoresponse under high intensity light. Obviously, only minor pulse shape changes are observed when the sensor photoresponse is linearly dependent on the pulse energy, whereas a pulse broadening from 7 to 12 ns is evident in the pulse energy region where the detector shows a sub-linear behavior on the light intensity. Even if trapping effects were found to slow down carrier transport close to the radiation damage threshold around 10 mJ $\cdot$ cm $^{-2}$ in diamond [31], for the results reported here the light intensity used during characterization was maintained to much lower energies. The observed photovoltage peak widening highlighted in figure 7 is a further confirmation of a gradual change from an initial monomolecular recombination mechanism, with carrier lifetime depending on the defect density, to a bimolecular one, as the irradiation intensity increases. Such a fact is further supported by the basically constant pulse response fall time in both $\beta = 1$ and $\beta = 0.5$ ranges. Conversely, the FWHM is affected by the progressive change in the recombination process also at low light fluxes.

4. Optically activated field effect transistors (OpFETs)

The ICT industry is focusing more and more on the development and optimization of devices based on wide bandgap semiconductors with high breakdown electric field, large saturation velocity values and noise immunity: all mandatory characteristics for devices operating in the high-frequency and

high-power output regimes. Besides, photonics is proposing applications requiring small dark current and highly selective response in the active spectral region. Photonic systems based on optically activated field effect transistors (OpFETs) provide key advantages over conventional electrically triggered fast electronic ones. The main desirable properties of such a phototransistor must be optical and electrical triggering gate, on–off controllability with a single optical monochromatic source, optical fiber coupling, high breakdown voltage, fast switching time and low on-state resistance. In 1980s GaInAs MESFETs were able to satisfy these requirements using detectors with notch structure and a 314 MHz mode-beating Nd:YAG laser at 1.06 μm [39]. The main limitation of such a kind of device was daylight sensitivity: indeed, solar blind behavior removes the need for screening devices [40] and for using more light optical guides with performance/weight ratio improvements. Such three-terminal devices, operating with majority-carrier, were able to detect light pulses of 100 ps duration with a 2 GHz repetition rate [41, 42]. The analytical modeling of the photo detection mechanism, the contribution of photogenerated charge carriers to the channel conductivity [43–46] and the noise factor [47, 48] have been investigated on enhancement mode GaAs MESFETs suitable to transform optical stimuli in electrical signals. Internal and external photogeneration regimes have been investigated: as the light intensity is varied, the open circuit voltage developed on the gate contact changes and a family of $I_{DS} - V_{DS}$ (V_{GS}) curves is obtained. In long channel MESFET the square root of the drain current, I_{DS}, is proportional to the incident power light logarithm when a fixed voltage V_{DS} is applied to the drain contact. Most solutions of such kinds of devices used the gate contact like a semitransparent photodiode. On the other hand, when UV radiation is concerned, the use of a wide bandgap semiconductor is mandatory. Looi *et al* [49, 50] were able to fabricate the first OpFET based on polycrystalline CVD diamond and found it suitable to operate with UV light. Such a device worked like a GaAs Schottky-gate FETs: i.e. as a photodiode in terms of turn-on characteristics and as a FET in terms of signal amplification. An optical gain $G = 4$ was measured at a wavelength of 200 nm. Since that time, mainly due to the difficulties in simulating the quasi-2D hole Fermi gas (2DHG) formed below the Schottky contact by diamond hydrogenation, no mathematical modeling of diamond OpFETs has been made available in the literature. The surface transfer doping model [51, 52] gives the basis to understand the surface conductivity in diamond as a consequence of a strong band bending and accumulation of subsurface holes in the diamond with a quasi-2D confinement. The surface conduction of these holes contributes to the formation of Schottky p-type junctions with some metals like aluminum, thereby giving the possibility to fabricate opaque-gate surface channel MESFETs. Shubha *et al* [53] and Alsunaidi *et al* [54] deeply investigated the modeling of opaque-gate devices on GaAs based structures. On the other hand, OpFET fabricated on hydrogenated diamond cannot be analyzed on the basis of these models because the quasi-2D hole accumulation and the apparent short channel effects. Figures 8 and 9 for example, show the I_{DS}–V_{DS} output

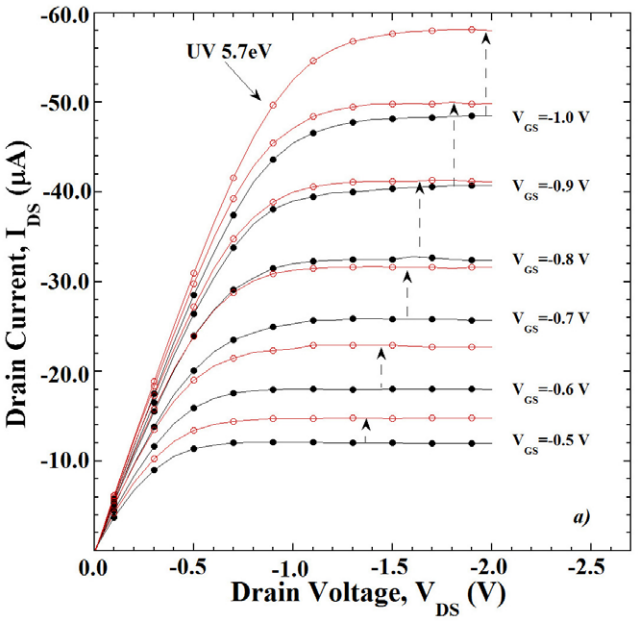

Figure 8. Response of an OpFET in the dark (black) and under 150 μW · cm^{-2} UV ($\lambda = 225$ nm) illumination (red). The arrows indicate the current increase under illumination at constant gate voltage V_{GS}. The device is fabricated on hydrogenated polycrystalline thermal grade diamond by Element Six. Aluminum and silver were used for gate and drain-source realization, respectively. Metals were 150 nm thick and gate dimensions were 50 μm in width and 4 μm in length. The device behaves like a p-channel normally-off transistor being the threshold voltage Vth $= -0.34$ V.

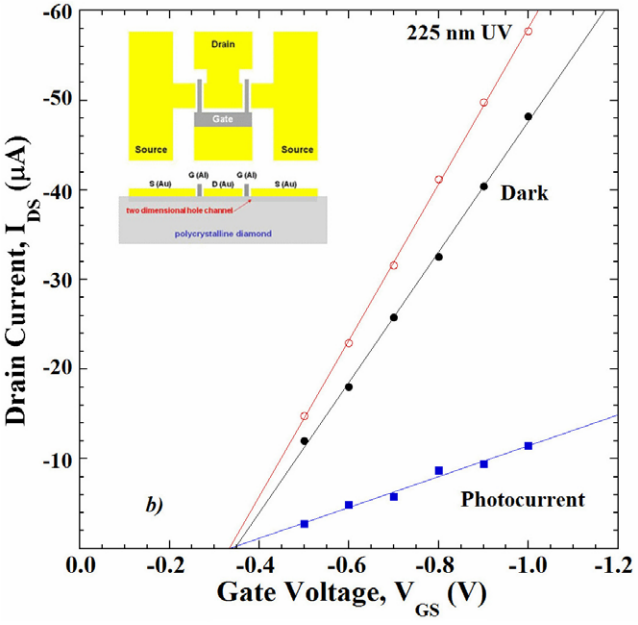

Figure 9. The linear increase of the current collected at the drain, I_{DS}, with the gate voltage, V_{GS}, in the saturation regime ($V_{DS} = -1.5$ V) both, in the dark and under illumination, demonstrates short-channel effects. It is worthwhile to observe the linear increase of the photocurrent amplitude.

characteristics of a device fabricated on small grain polycrystalline diamond and I_{DS} dependence on the gate voltage, V_{GS}, in the dark and under UV illumination [55].

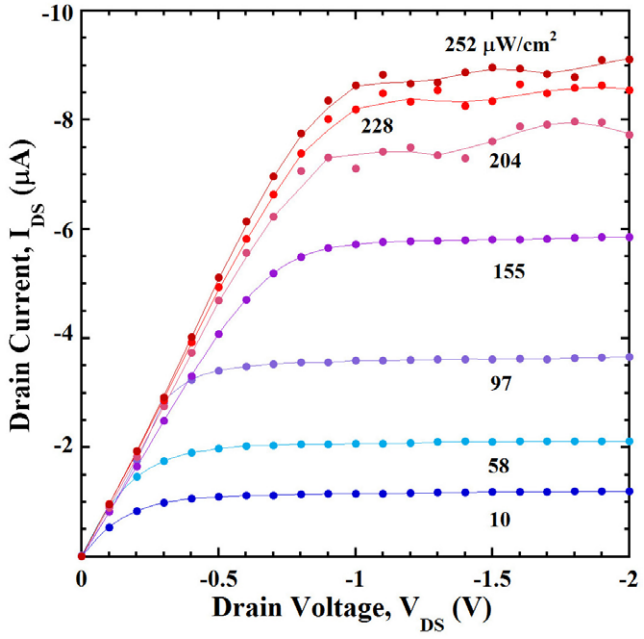

Figure 10. Current collected at the drain contact, I_{DS}, versus the drain voltage, V_{DS}, maintaining the gate contact floating. The measurement has been carried out under 225 nm UV radiation illumination with different power densities. In the I_{DS}–V_{DS} saturation regime, a linear increase of the current amplitude on the incident light power density is observed.

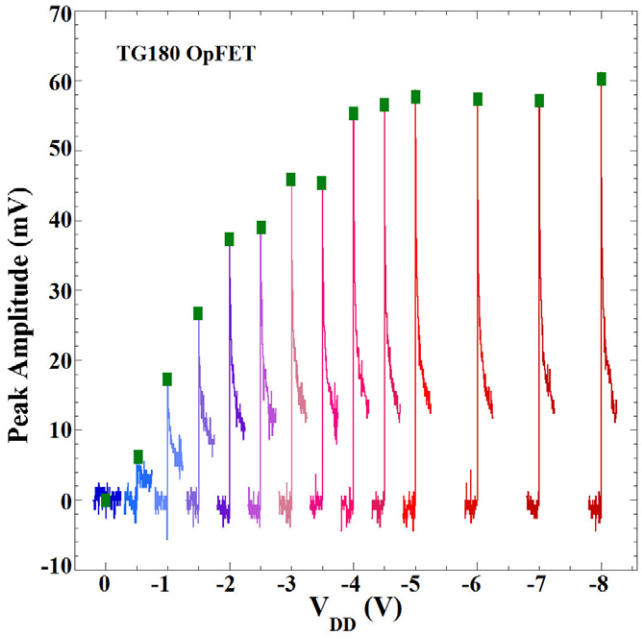

Figure 11. Peak amplitude versus voltage V_{DD} applied to the drain contact through a Picosecond 5575A bias tee for a constant gate voltage $V_{GS} = -3.4$ V. The laser was a Neweks PSX-100, 193 nm, 10 Hz, 4.5 mJ per pulse. A silica lens, $f = 10$ cm, was inserted at the laser output. The photocurrent amplitude was measured as the voltage signal across the 50 Ω input impedance of a LeCroy Wavepro 960 digital sampling oscilloscope. Green dots are a visual aid to localize the peak maximum.

The channel conductance, g_D, increases rapidly with V_{GS} highlighting an enhancement mode behavior. Leakage current at $V_{GS} = 0$ is of few pA. The UV light clearly enhances the channel conductance and g_D changes between 40 μS and 70 μS and approaches the pinch-off condition for values around $V_{DS} = -1.5$ V at $V_{GS} = -1$ V. As clearly evidenced in figure 9, the photocurrent linearly increases with V_{GS} leading to a constant g_m transconductance value, with an improvement from 18 mS · mm^{-1} in the dark to 22 mS · mm^{-1} under illumination. In contrast, the threshold voltage $V_{th} = -0.34 \pm 0.01$ V remains constant.

Figure 10 shows the response to different UV beam power densities with the gate left floating. Due to the device geometry and the aluminum gate thickness, charge carrier generation is possible only in between the H-terminated gate-drain region, estimated to have a 200 μm^2 area. The device response shows initially a constant channel conductance $g_D = 10$ μS up to $V_{DS} = -0.5$ V, thus initiating a decrease reaching the channel pinch-off. Channel length modulation appears at higher powers. The charge carrier density inside the channel linearly increases with the UV beam power intensity. This trend addresses the device to act as a simple photoconductor in the saturation regime. At the wavelength used, charge carriers, generated in the exposed gate-source and gate-drain volumes (i.e. about 400 μm^2 in the area and within few microns in the depth from the surface) can diffuse below the gate (holes) while it is expected that most part of electrons are swept-out by the electric field to the body back contact. Holes collected in the channel contribute to the improvement of band bending thereby increasing with the beam intensity. Notwithstanding the presence of grain boundaries with their recombination attitude, enough photogenerated holes can diffuse and produce the same effect gained by an applied bias voltage, enabling an increase of the current flow. Opaque gate OpFETs were also fabricated on very smooth freestanding 110 μm thick hydrogenated diamond films and the response to 200 nm UV light has been studied [56, 57]. The results under continuous UV illumination underlined the typical characteristic of enhancement-mode MESFETs.

Phototransistors were also fabricated on commercial thermal grade plates [58] and studied using pulsed UV laser light. In [59] an OpFET has been reported in which the accumulation layer was absent between the gate and drain zones and a nanosecond pulsed 193 nm ArF excimer laser was used to enhance the charge carrier accumulation in such a channel to switch-on the device. In such an OpFET, hydrogenation was limited to the source-to-gate region, whereas the active device area was the gate-to-drain one demonstrating fast switching performances. Figure 11 depicts the transient response at different drain voltages for a constant gate bias $V_{GS} = -3.4$ V. Increasing the voltage applied to the drain contact via a bias-tee used for oscilloscope coupling, the signal initially increases up to the $V_{DD} = -3.5$ V value. In such a case, the electric field in the gate-drain region approaches zero, so that a peak amplitude current signal saturation is observed. In order to improve charge photogeneration mainly within the gate-drain region an asymmetric structure was implemented for device fabrication [60]. Figure 12 reports the scheme of such a device with a micrograph showing the interdigitated electrode's architecture. In [61] the analysis of this asymmetric OpFETs in the

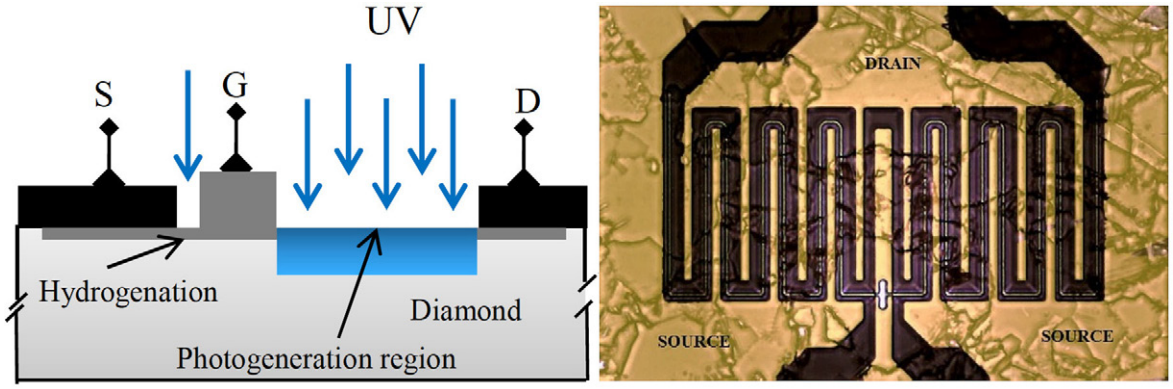

Figure 12. Scheme of asymmetric gate design on hydrogenated polycrystalline diamond aimed to improve the photogeneration area mainly within the gate-drain region (on the left) and optical microscope view of one of the developed OpFET devices with maximized sensitive area (on the right).

dark and under 193 nm ArF excimer laser irradiation is discussed. The results showed that when the drain is left floating, no charge can be collected at the drain contact and no current is revealed in the output load (represented by the low input impedance of the oscilloscope). The drain voltage increase enhances charge accumulation at the drain contact leading to a larger signal (see figure 13). The output pulse shape remained almost the same with a FWHM equal to 9 ns. The rise time was larger than that observed in experiments performed changing the gate control voltage. Authors ascribed the difference to the longer time constant caused by the pull-up 100 kΩ drain resistance value. Due to the thin layer of diamond involved in the charge photogeneration and transistor effect, requirements for fast switching and sensitive response appear to be limited to the average grain size and hydrogenation level both influencing the charge mobility. Very fast response to ArF excimer laser irradiation in the nanosecond regime and the sensitivity to gate and drain voltage variations demonstrate the suitability of these architectures for applications in emerging photonics technologies able to work as fast switching optical receivers.

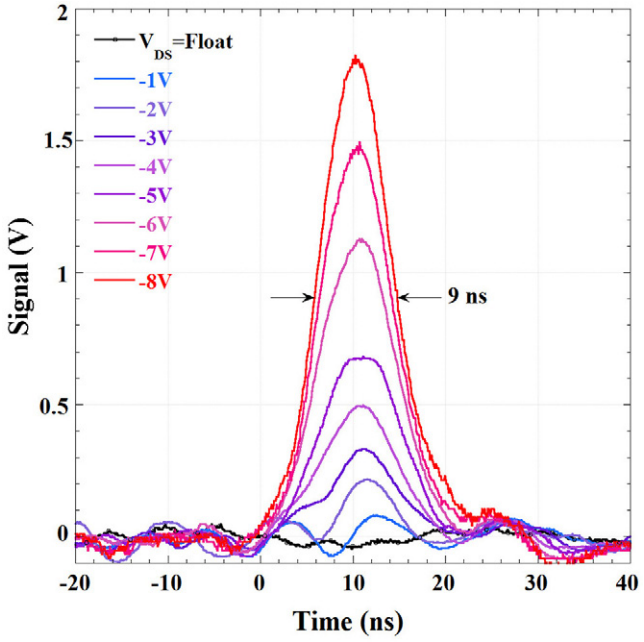

Figure 13. Transient response of an asymmetric OpFET to 193 nm laser pulses monitored when the gate control voltage $V_{GS} = -2$ V as a function of the voltage V_{DD} applied to the pull-up 100 kΩ resistance. Dimensions: $W_G = 200$ μm; $L_G = 4$ μm; $G - D = 12$ μm; $G - S \sim 1$ μm.

5. Position sensitive detectors

The general name of position sensitive detector (PSD) includes a wide range of components able to produce an output signal dependent on the impinging beam position, independently of the basic principle governing the device performance. A first class relates to discrete sensors: mono or bi-dimensional array of discrete light-sensing elements (as photodiode array or charged coupled device, CCD) can be effectively used for beam position detection. As elucidated in the next section, discrete sensors are able to give information on both the beam position and the intensity beam profile, so that they become really useful in fields where the incident light-spot shows an irregular shape. As drawbacks, a pixelated sensor shows a relatively high device cost, together with a cost increase due to the complexity of the readout electronics, to be connected to each pixel, and the required processing of the acquired signals. Such a complexity may also limit the detection speed: a low speed device will be inadequate as the feedback component of an automatic light-alignment control system. In the same class of discrete sensors we can also include the so called 'segmented PSDs', which refer to devices where the sensor surface is generally patterned in just two or four segments, to obtain respectively 1D or 2D sensitivity [62]. Information about the position is obtained by simply comparing the signal acquired on each cell. In such a class, four-quadrant sensors are used to accurately measure the displacement of an incident beam relative to the calibrated center. These devices are ideal for measuring the movement of a beam, the distance traveled by an object, or as feedback sensing elements for alignment systems in optics. The best response is obtained when all four sensing elements give the same signal, corresponding to a beam impinging on the center of the device. However, the element response strongly depends on the beam size and light uniformity, so that they can only be used in systems where the beam

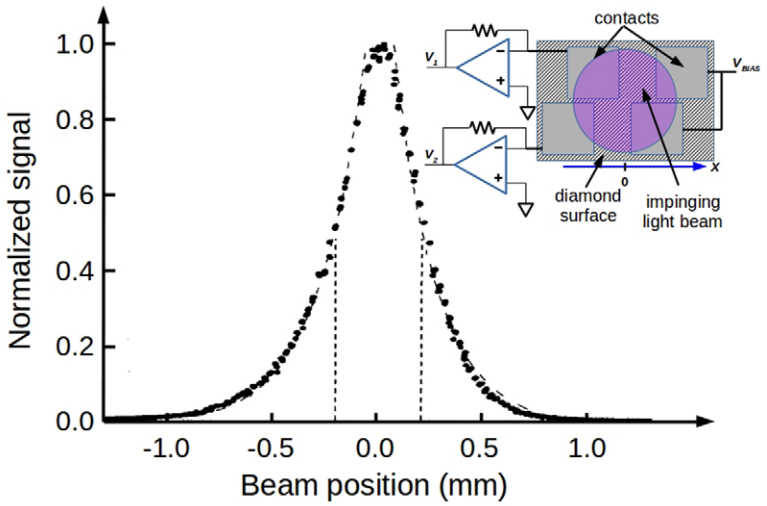

Figure 14. Photocurrent signal of a simple diamond PSD versus the relative distance between the spot light and the active area of device. Very high sensitivity is gained at ± 200 μm, with respect to the central position, and induced by the gaussian shape of the light spot. The inset shows a sketch of the sensor layout. Transimpedance amplifiers are used for the detector interface towards the acquisition electronics.

must be kept in an exact position. However, as the magnitude of the beam displacement is unknown, the time needed to realign the light spot can be too long for time critical applications. It is noteworthy that the segmented structure presents a quite large degree of freedom in the design, as each cell can be realized as a photoconductor, a photodiode or any other kind of photodetector structure: this has already allowed the realization of diamond based four-quadrant PSDs, as planar structure for UV radiation [63], or as sandwich detectors for x-ray and synchrotron light sources (see Bergonzo *et al* [64]).

Overcoming the lack of p-n junction fabrication, a very simple way to realize a 1D diamond based PSD is that depicted in the inset of figure 14 [65]. Here the current signals collected at metal contact are converted as voltage and the beam position is given by the $(V_1 - V_2)/(V_1 + V_2)$ ratio. In addition, due to the total $V_2 + V_1$ signal normalization, such a double-sensor configuration would be insensitive to light beam intensity variations. Data reported in figure 14 were related to the V_1 signal alone. The maximum sensitivity (signal variation induced by light beam displacement) was observed when the spot is shifted by 200 μm from the sensor center where high sensitivity was assured by the gaussian shape of light spot intensity.

The above mentioned structure can be extended to realize a planar two-dimensional PSD based on a four-quadrant pattern for surface contacts. Figure 15 reproduces the layout of such a planar sensor in which four interdigitated contacts represent the device quadrants, whereas figure 16 reports the typical behaviors of the relative photocurrent signals of two adjacent quadrants.

Pixelated and segmented devices, together with beam displacement, also allow information to be gained on the intensity of light impinging on a single sensing element. Conversely, when the positional sensitivity plays a major role, one can refer to the so called *continuous PSDs*. These devices allow continuous position data and faster signal elaboration, usually displaying a high position resolution [66]. Continuous PSDs are usually based on a p-n homojunction with a high conductivity layer grown on a substrate with a lower conductivity and an opposite doping. This structure represents one of the major applications of the lateral photovoltaic effect reported by Schottky in 1930 [67], next rediscovered by Wallmark in 1957 [68], who applied it for the first position sensing device, in monocrystalline germanium, and simply extended to the case of structures based on Schottky junctions [69]. Silicon-based PSD technology is well established and sensors show very good performances, with a typical nonlinearity lower than 1% at a relatively low cost. Conversely, moving toward diamond as the active material, due to the lack of an efficient n-type doping, it is impossible to simply reproduce the same p-n junction based technology. For diamond several research groups claim to have obtained a n-type conduction in diamond [70, 71] and to have realized p-n junctions and LEDs [72]. Anyway the technology has not appeared mature enough yet to allow the realization of bipolar devices. An alternative way may implement the well studied p-type surface conductivity of hydrogen-terminated diamond [51] to realize Schottky junctions [73, 74], but problems arise in the hydrogenated layer stability when high peak power irradiation, typical of the excimer lasers, is concerned. A simple way for one- or two-dimensional diamond-based PSD realization consists on the deposition of a resistive layer equipped with two metallic charge collection electrodes on the diamond surface. As resistive material either a thin, semitransparent metal or a DLC layer can be used. Applied bias voltage drives photogenerated charge carriers towards the peripheral collecting electrodes. The light spot position is then reconstructed taking into account charge division between the two electrodes: collected currents are normalized to the total current signal and will be proportional to the detector length along the respective axis. For example, such a solution has been recently adopted for particle beam monitoring [75]. To evaluate the feasibility of a method of this kind, a very simple voltage-division (VD) approach have been previously adopted for a diamond PSD [76]. A detailed analysis can be used to optimize device performances in terms of just two main system parameters: the resistance value of the layer used for voltage partitioning and the equivalent output resistance seen by the acquisition

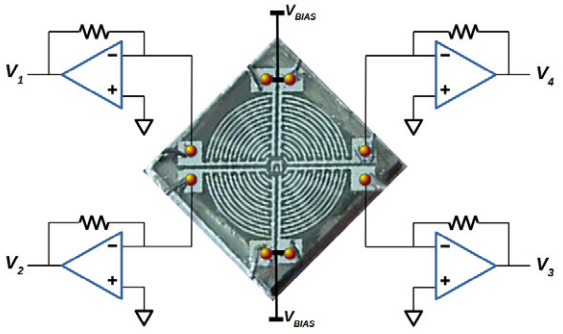

Figure 15. Four-quadrant metal–diamond–metal planar structure used for UV beam position monitoring. Photocurrent signals, converted as $V_1 - V_4$ voltages, are processed to evaluate the light spot displacement position with respect to the sensor center.

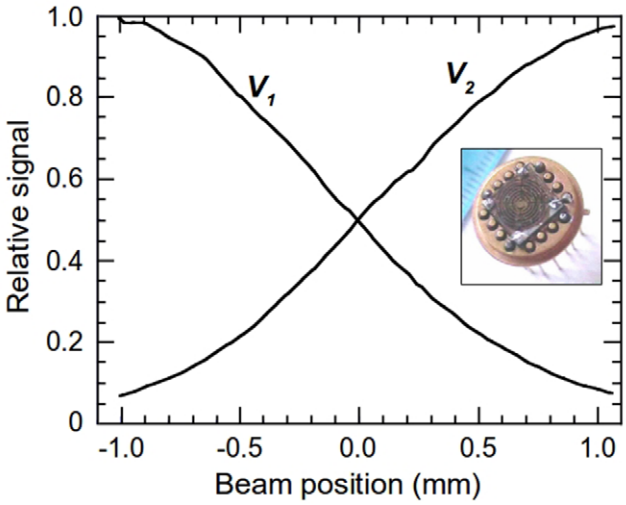

Figure 16. A typical cross-over characteristics of two adjacent quadrants of the sensor depicted in figure 15. In the inset, the picture reproduces the diamond detector mounted on a standard chip-holder used to simplify the device characterization.

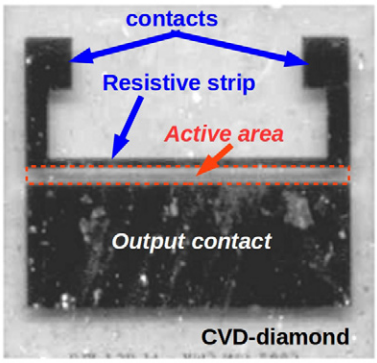

Figure 17. Voltage-division diamond PSD. Thin Cr deposition has been used for the resistive strip realization, whereas silver pads are used for external connections.

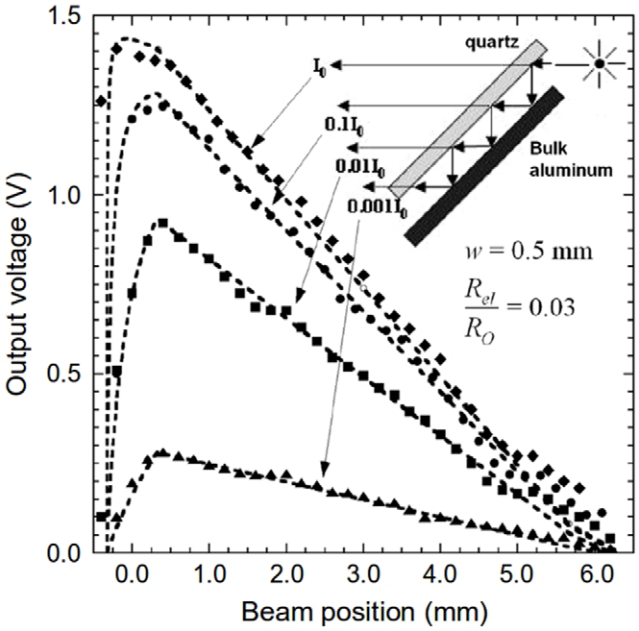

Figure 18. VD-PSD output signal for different intensities of the incident laser light. Dotted lines show the best fit results according to the simple model discussed elsewhere [77]. The inset shows the scheme adopted to generate four beams obtained by multiple reflection across a quartz plate faced to a bulk aluminum mirror. The intensity lowering on each output beam is about one order of magnitude.

electronics [77]. Figure 17 shows a polycrystalline diamond 1D VD-PSD where chromium has been used for the resistive strip line. To evaluate VD-PSD sensitivity on the beam light intensity (ultraviolet pulsed ArF-excimer laser, Neweks PSX100, 193 nm, 10–100 Hz pulse repetition frequency, and nominal 3 ns of FWHM) the laser light was attenuated by means of multiple reflections across a quartz plate faced with a bulk aluminum mirror (see the inset in following figure 18). The obtained four beams are separated by one order of magnitude in intensity of each other. The experimental results of the performed characterization are reported in figure 18. Dotted lines relate to best fit results according to theoretical analysis [77]. Experimental results confirmed the feasibility of a VD-PSD for UV-laser beam position diagnostics in which a non-linearity of a few percentages on the peak amplitude was easily gained.

6. Pixel architectures

In the last decades, excimer laser beam profiling has gained increasing attention both in the scientific and industrial world, owing to the importance that the use of sub-250 nm laser wavelengths have taken on in a wide range of application fields. A first significant example can be found in ULSI microelectronics technology, where 193 nm ArF lasers are still commonly used for photolithography purposes [34], pushing the resolution limit down to 22 nm thanks to the use of adaptive optics, immersion lithography and other frontier techniques, such as double-patterning. High-power, short-pulse UV excimer laser technology is also extensively used for producing fine features and structures in micromachining [78]. Finally, excimer lasers revolutionized the world of eye surgery, by introducing the possibility of correcting common refractive errors of the eye, such as myopia, through photorefractive keratectomy (PRK) or laser assisted *in situ* keratomileusis (LASIK) [35]. In all of these applications, a real-time monitoring of the spatial intensity profile of the laser spot is

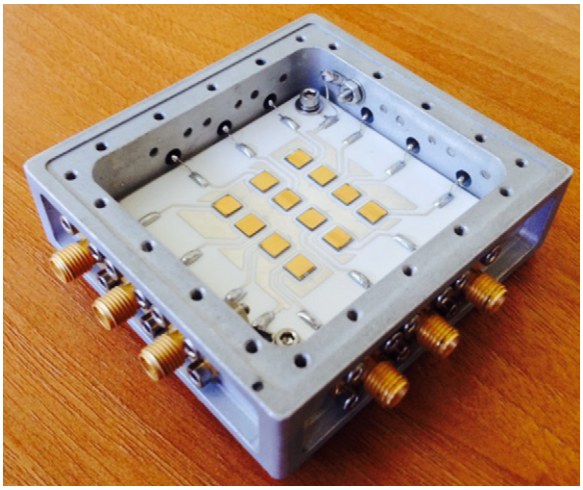

Figure 19. Prototype of a 12 pixel mosaic diamond detector used for neutron beam monitoring and spectroscopy. Each pixel is made up of a single-crystal diamond sample of the highest quality ('electronic grade'), allowing for energy resolution to be <2%.

crucial to ensure reproducibility of the ongoing process and, in the case of surgery, also for safety purposes. The market of excimer laser beam profiling systems is currently dominated by CCD cameras based on UV-enhanced silicon, due to the well-established technology of silicon and the possibility of exploiting a very large number of pixels (up to the megapixel range), thus improving significantly the spatial resolution (down to the μm range). Problems related to the very high UV absorption in silicon, leading to a very low penetration depth (few nm) of the impinging light, and consequently to the risk of absorbing radiation in the gate material rather than generating a photoelectric signal within the channel of the CCD, have been solved following several approaches: (1) by the deposition of UV-sensitive phosphor coatings [79, 80]; (2) by using a backside-thinned back-illuminated CCD design [81]; (3) by using a deep-depletion CCD structure, where a lightly doped substrate is used to extend the depletion region, normally under the CCD gates, to the back of the wafer [82]. However, despite the excellent resolution obtainable, all of these approaches have several major drawbacks when dealing with high-power, high-fluence sources as excimer lasers, mostly due to the very low radiation hardness: significant degradation after a relatively low number (about 5×10^5) of low-energy (10 pJ) incident pulses have been observed, for example, with F_2 lasers ($\lambda = 157$ nm) [83], forcing silicon cameras to adopt attenuators and/or wavelength converters to limit the damages induced by radiation. Such a switch from direct to indirect imaging unavoidably introduces some losses in information on the radiation intensity, and surely increases the complexity of the overall imaging system, as well as its cost. Diamond could represent a valid alternative to silicon for the development of pixel detectors for excimer laser beam profiling, owing to its peculiar optical, electronic and chemical properties (see sections 1 and 3): in particular, with respect to conventional semiconductors, the solar blindness and the excellent radiation hardness allow for direct imaging of high-power UV sources with no need for wavelength converters or attenuators.

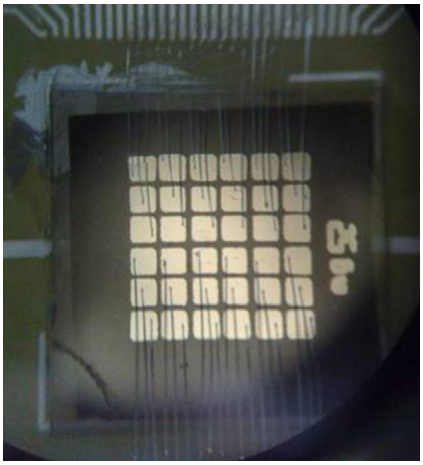

Figure 20. 36 pixel detector fabricated on a 10×10 mm^2 polycrystalline diamond sample. Each pixel is wire-bonded to its own signal channel (copper track on a PCB) by an Al/Si wire.

Another advantage of exploiting diamond technology for excimer laser beam profiling is that diamond detectors act as photoresistances (or photodiodes, depending on the metal contacts used), making the fabrication of the devices quite simple if compared to the complexity of CCD silicon-based technology. Pixel detectors require basically only deposition and patterning of metal electrodes on the top and bottom surfaces of the diamond substrate. Also, the possibility of using polycrystalline diamond as a substrate material makes diamond technology cost-effective, due to the improvement and refinement of deposition techniques of reproducible polycrystalline films, which are now available on the market at a very competitive price. Single-crystal diamond plates would indeed be more appealing than polycrystalline substrates, due to their better electronic properties, but are limited by the restricted lateral dimensions achievable (up to about 4.5×4.5 mm^2): this forces multiple substrates to be used to cover large detection areas, building up 'mosaic' detectors, such as the one shown in figure 19. However, this solution is quite expensive, and is reserved to niche applications such as neutron and alpha spectroscopy [13, 84, 85], where the use of crystals with a 100% charge collection efficiency is mandatory to achieve a 'spectroscopic grade' energy resolution (<5%), not obtainable with polycrystals [86]. On the other hand, polycrystalline diamond substrates are perfectly suited to act as active materials for the realization of pixel detectors for UV laser beam imaging. In the past few years, several works have been published in the literature, introducing prototype pixel detectors which showed very good results in real-time monitoring of UV sources, both continuous and pulsed. Figure 20 shows a 36 pixel prototype fabricated on a 10×10 mm^2, 270 μm thick polycrystalline sample, provided by the General Physics Institute, Russian Academy of Sciences, with average lateral dimensions of the grains of 200 μm. Metal contacts were fabricated by Ag evaporation on the top and bottom surface of the sample: thickness of the bottom electrode, used for device biasing, was only 50 nm, in order to ensure semi-transparency to the UV light impinging on the back (figure 21), whereas the top contact structure was 200 nm thick. Standard photolithography was finally performed to define the

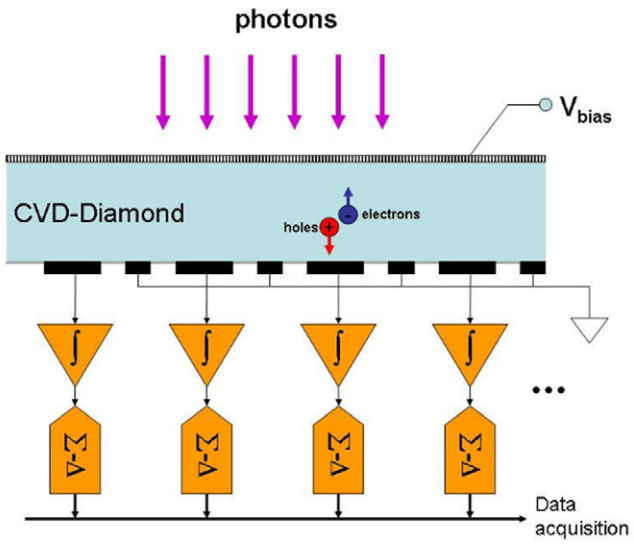

Figure 21. Operating principle of a diamond pixel architecture for UV laser beam and ionizing radiation monitoring. Pixel contacts can be surrounded by a metal guard-ring connected to the ground to drastically reduce crosstalk.

36 pixel array structure (750×750 μm^2 each, 150 μm apart). The operating principle of the pixel diamond detector is very simple. The energy of the photons impinging on the semi-transparent contact is absorbed by the detector bulk, and converted to electron–hole pairs: a transverse electric field allows for the separation of photogenerated carriers and their drift towards the collecting electrodes. Each pixel current signal is conditioned by a dedicated front-end electronics, made up of a high-precision switched capacitor integrator and a high-resolution $\Sigma - \Delta$ analog-to-digital converter. The overall system is able to provide up to 2000 samples per second (SPS) allowing for real-time UV-beam monitoring in most practical uses. The beam-profiling system is also equipped with a microcontroller-based computer-interfaced main board for data acquisition and transfer. It is worthwhile to mention here that the design of a dedicated electronics is mandatory for diamond devices, due to the peculiar characteristics of the photocurrent signal: in particular, being dark current in the pA range (with signals reaching few nA at most), a commercial transimpedance amplifier, as the ones commonly used for other semiconductor-based detectors, could be completely ineffective, due to its noise current lying in the range of the signal amplitude to be measured. The pixel detector shown in figure 20 was first tested to verify its ability to give information on the profile of UV incoherent light sources [87]. Figure 22 shows the profile of a monochromatic UV light source ($\lambda = 235$ nm, 5×5 mm^2 spot-size, 1 μW $\cdot$ cm^{-2} intensity) selected at the output of a double spectrometer coupled to a 300 W arc-discharge Xe-Hg lamp. The pixel detector was mounted on a micrometric *X*–*Y* moving stage with 10 μm resolution. A 500 μm wide pinhole was used for calibration purposes, necessary to compensate for inter-pixel dispersion. The calibration procedure started with the alignment of the spot centroid over the first pixel; successive translations along the *X*–*Y* directions, by steps equal to the inter-pixel distance, allowed for the evaluation of the normalization factors to take into account during the 'parallel' real-time acquisition. After calibration, UV spotlight was positioned on the center of the detecting area: starting from this position and keeping *Y* coordinate constant, subsequent 250 μm-step translations along the *X* axis were made, performing a real-time acquisition of the beam profile at each step. The same pixel detector prototype as the one employed for UV lamps was used for excimer laser beam profile measurements [88] with an ArF laser ($\lambda = 193$ nm, 4.5 mJ pulse peak energy, $10 \div 100$ Hz repetition rate): no form of attenuation was adopted, in order to test the detector performance under high-power high-fluence conditions. The beam profile shown in figure 23 is relative to a single excimer laser pulse: diamond outstanding properties in terms of photoresponse speed and read-out electronics high throughput allowed for single pulses to be collected and processed one by one, even at high repetition rates. Moreover, pixel detector radiation hardness was tested up to a fluency of 1.4 mJ $\cdot$ cm^{-2}: neither radiation damage nor performance drop-off were observed, even after $2 \cdot 10^6$ pulses, thus showing a significant lifetime improvement over silicon CCD cameras [83].

After the completion of the prototyping stage, research activity on diamond-based pixel architectures focused in recent years on different targets, especially on the refinement of the properties of the collecting electrodes. Girolami *et al* [89] showed that a Ti/Au multilayer contact structure can lead to a remarkable improvement of the detector sensitivity with respect to Ag contacts, paving the way to a pixel density increase and to the development of more accurate beam profilers. Another goal is the improvement of the stability of the ohmic contacts, aimed at increasing the resistance to radiation damage of the collecting electrodes. In this sense, Pacilli *et al* [90] proposed metal-less graphitic contacts fabricated on polycrystalline diamond samples by laser-induced graphitization: a 36 pixel detector was fabricated and tested under a ^{90}Sr beta radioactive source, showing very good performance in terms of signal stability and pixel response uniformity. Also, the definition of pixel structures by direct laser writing highlights the possibility in general of avoiding metal patterning through complex lithographic processes, thus further simplifying diamond technology for pixel architectures. It must be stressed here that the simple operating principle of a pixel diamond detector, acting in a few words as a 2D array of photoresistances, makes the same device suitable to monitor a wide range of sources, from UV excimer lasers to x-rays, from neutrons to charged particles. What makes the difference between one application and another is the front-end electronics, which must be properly designed and tailored to the features of the source to be profiled: for instance, the possibility of selecting the integration time *T* and the input charge range *Q* of the current-input preamplifier can sensibly extend the intensity measurement range, making the device useful to profile both sources producing large signals (low *T*, high *Q*), such as excimer lasers or x-ray tubes, and weak sources (high *T*, low *Q*), such as radioactive isotopes with activity as low as a few kBq. Moreover, the selectable number of acquisitions may significantly improve the measurement accuracy in the case of weak and/or noisy sources, and gives additional diagnostic information such as the spot centroid position, the mean and maximum intensity values, and the beam displacement from a reference position.

In conclusion, diamond pixel architectures demonstrated to be a versatile solution for UV laser monitoring, as well as for

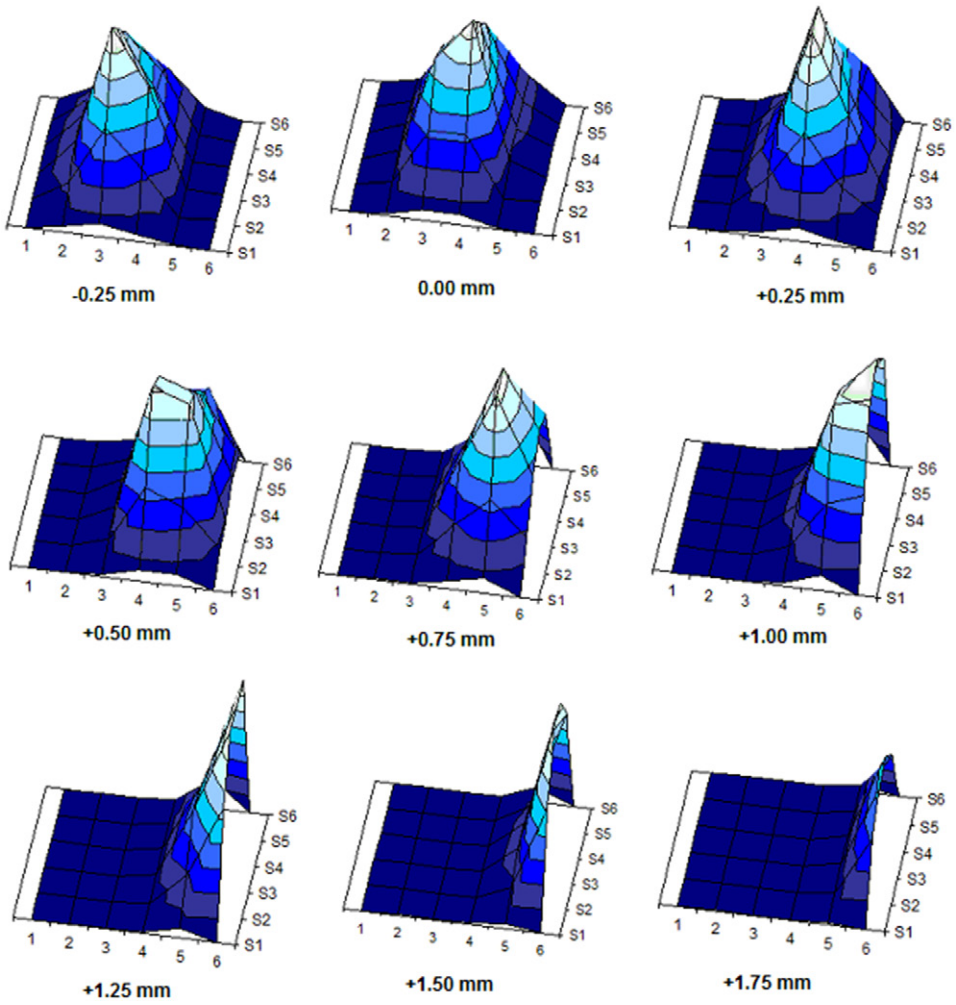

Figure 22. 3D beam profiles of a UV Xe-Hg lamp. Relative displacements from the starting positions were also indicated.

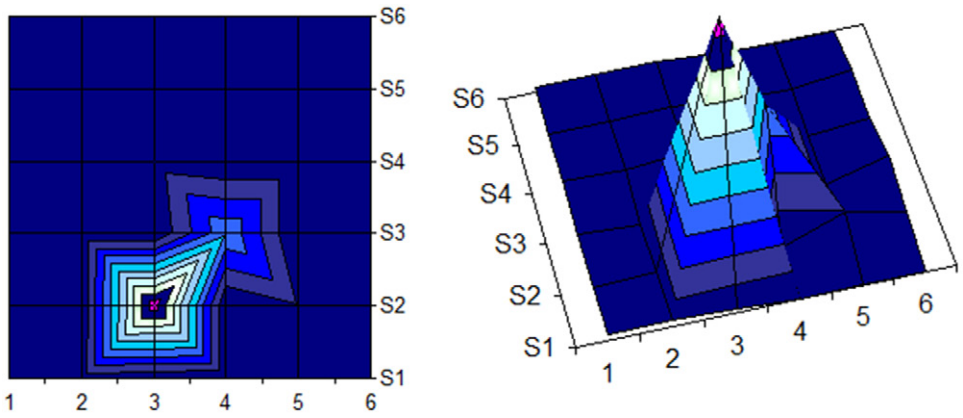

Figure 23. Beam profile of a single excimer laser pulse (ArF): top view (left) and 3D view (right). Spatial dimensions of the profile were 5.25×5.25 mm^2.

profiling of other UV sources and ionizing radiations. Major benefits with respect to common silicon-based CCD cameras have to be found in the possibility of performing a direct imaging without attenuators or converters placed between the source to be monitored and the device, and in the outstanding radiation hardness that allows for the lifetime of the detector to be extended well beyond the limits of conventional beam profilers. However, diamond devices have some drawbacks that hamper their extension to large scale as high-resolution UV beam profilers. The number of pixels will always be limited (up to a few hundreds maximum) by the impossibility of adopting a CCD technology; moreover, an increase in the number of pixels, due to the limited lateral dimensions of diamond substrates ($\sim 2 \times 2$ cm^2 in case of polycrystals), would be most probably obtained at the expense of a lower sensitivity, because the pixel area would be unavoidably reduced.

Conversely, when high-resolution is not crucial and a direct measurement of the intensity profile of high-power high-fluence sources is required, diamond pixel detectors could definitely be considered the first choice.

7. Summary and conclusions

While excellent semiconducting properties of diamond, attractive to detector applications, have been known for a long time—since the use of natural diamonds for this purpose [91]–the impressive development of ionizing particles, x-ray and UV sensors took place only with the progress in the growth of high quality CVD diamond in the last two decades. Single crystal diamonds with nitrogen impurity content at the 1 ppb level and even below, not available in nature, yet still of limited size (typically, less than 10 mm), can now be produced by CVD technique, and are quite appropriate to build the radiation hard detectors. On the other hand, large-area, more than two inches in diameter, polycrystalline CVD diamond wafers, while having a little bit lower electronic properties, allow realization of pixel detectors for on-line UV beam monitoring and imaging, as was described above. There is a hope that the dream on a combination of single crystal perfection with large area for advanced detectors will be realized by using 'mosaic' substrates, composed of a number of identical plates 'fused' by CVD diamond 'solder'. An impressive example of such mosaics of 40×60 mm^2 in size, consisted of 24 SC diamond plates 10×10 mm^2 in area each has been reported recently by Yamada *et al* [92]. In a broader context the links of CVD diamond and lasers, besides considered here UV detectors, include, in particular, diamond optics for high power cw IR lasers [93–95], diamond heat spreaders in watt-level power semiconductor disk lasers [96], and exciting emerging application related to the development of compact high power diamond Raman converters [97]; and diamond Raman lasers (DRL) [98] with the recent demonstration of DRL cw performance at powers above 100 W [99]. Also, a feedback from laser processing technology is important for introducing a new architecture and structure of contacts, in particular surface graphitic contacts prepared by UV KrF excimer laser ablation of diamond [90]. It is appropriate to remind here that historically the first study of laser treatment of polycrystalline CVD diamond films, to our knowledge, was performed at the GPI RAS in 1988 under encouraging support of Professor Alexander Prokhorov [100], and still the 'diamond-laser' couple brings a rich harvest, including the recently demonstrated novel three-dimensional radiation detectors with a regular array of buried pillared electrodes formed in diamond bulk by a femtosecond laser-induced phase transition of diamond to graphite [101, 102].

Acknowledgments

A part of this work on laser-assisted graphitic contacts formation was performed with financial support of Ministry of Education and Science of Russian Federation, Agreement No. 14.579.21.0030, the unique identifier RFMEFI57914X0030.

References

[1] Kalish R, Reznik A, Prawer S, Saada D and Adler J 1999 *Phys. Status Solidi* a **174** 83–99
[2] Gracio J J, Fan Q H and Madaleno J C 2010 *J. Phys. D: Appl. Phys.* **43** 374017
[3] Isberg J, Hammersberg J, Johansson E, Wikström T, Twitchen D J, Whitehead A J, Coe S E and Scarsbrook G A 2002 *Science* **297** 1670–2
[4] Pomorski M, Berdermann E, Caragheorgheopol A, Ciobanu M, Kiš M, Martemiyanov A, Nebel C and Moritz P 2006 *Phys. Status Solidi* a **203** 3152–60
[5] Collins A T 2009 *CVD Diamond for Electronic Devices and Sensors* ed R S Sussmann (New York: Wiley)
[6] Salvatori S, Vincenzoni R, Rossi M, Galluzzi F, Pinzari F, Cappelli E and Ascarelli P 1996 *Diam. Relat. Mater.* **5** 775–8
[7] Salvatori S, Rossi M, Galluzzi F and Pace E 1997 *Mater. Sci. Eng.* B **46** 105–11
[8] Salvatori S, Rossi M C and Galluzzi F 2000 *IEEE Trans. Electron Devices* **47** 1334–40
[9] Spaziani F, Rossi M C, Salvatori S, Conte G and Ascarelli P 2003 *Appl. Phys. Lett.* **82** 3785–7
[10] Yamada H, Chayahara A, Mokuno Y, Umezawa H, ichi Shikata S and Fujimori N 2010 *Appl. Phys. Express* **3** 051301
[11] Vikharev A L, Gorbachev A M, Dukhnovsky M P, Muchnikov A B, Ratnikova A K and Fedorov Y Y 2012 *Semiconductors* **46** 263–6
[12] Mokuno Y, Kato Y, Tsubouchi N, Chayahara A, Yamada H and Shikata S 2014 *Appl. Phys. Lett.* **104** 252109
[13] Girolami M, Bellucci A, Calvani P, Cazzaniga C, Rebai M, Rigamonti D, Tardocchi M, Pillon M and Trucchi D M 2015 *Phys. Status Solidi* a **212** 2424–30
[14] Sze S M and Ng K K 2006 *Chapter 13—Physics of Semiconductor Devices* 3rd edn (New York: wiley)
[15] Salvatori S, Rossi M C and Galluzzi F 1999 *Carbon* **37** 811–6
[16] Nesládek M, Vaněček M, Rosa J, Quaeyhaegens C and Stals L 1995 *Diam. Relat. Mater.* **4** 697–701 (diamond films '94)
[17] Rossi M, Salvatori S and Galluzzi F 1997 *Diam. Relat. Mater.* **6** 712–6
[18] Salvatori S, Rossi M C, Scotti F, Conte G, Galluzzi F and Ralchenko V 2000 *Diam. Relat. Mater.* **9** 982–6
[19] Salvatori S, Scala A D, Rossi M and Conte G 2002 *Diam. Relat. Mater.* **11** 458–62
[20] McKeag R D, Marshall R D, Baral B, Chan S S M and Jackman R B 1997 *Diam. Relat. Mater.* **6** 374–80
[21] Mazzeo G, Salvatori S, Rossi M C, Conte G and Castex M C 2004 *Sensors Actuators A: Phys.* **113** 277–81
[22] Ralchenko V G, Saveliev A V, Konov V I, Spaziani F and Conte G 2006 *IEEE J. Quantum Electron.* **36** 487
[23] Nunnally W and Hammond R 1984 {CH.} 12—optoelectronic switch for pulsed power *Picosecond Optoelectronic Devices* ed C H Lee (London: Academic) pp 373–98
[24] Ho P T, Lee C, Stephenson J and Cavanagh R 1983 *Opt. Commun.* **46** 202–4
[25] Bharadwaj P K, Code R F, van Driel H M and Walentynowicz E 1983 *Appl. Phys. Lett.* **43** 207–9
[26] Panchhi P and Driel H 1986 *IEEE J. Quantum Electron.* **22** 101–7
[27] Garnov S V, Klimentov S M, Pimenov S M, Konov V I, Kononenko V V, Tsarkova O G, Gloor S, Luethy W A and Weber H P 1998 *Proc. SPIE* **3287** 67–77
[28] Ho P T, Peng F and Goldhar J 1990 *IEEE Trans. Electron Dev.* **37** 2517–9
[29] Aikawa Y, Baba K, Shohata N, Yoneda H and Ueda K 1996 *Diam. Relat. Mater.* **5** 737–40
[30] Konov V I, Kononenko T V and Kononenko V V 2013 *Laser Micro- and Nanoprocessing of Diamond Materials* (New York: Wiley) pp 385–443

[31] Whitfield M D, Lansley S P, Gaudin O, McKeag R D, Rizvi N and Jackman R B 2001 *Diam. Relat. Mater.* **10** 715–21
[32] Yoneda H, Tokuyama K, ichi Ueda K, Yamamoto H and Baba K 2001 *Appl. Opt.* 40 6733–6
[33] Xu X, Schein J, Qi N, Prasad R R, Krishnan M, Fumihiko T and Tantawi S G 2001 *IEEE Trans. Plasma Sci.* **29** 85–92
[34] Gower M C 2000 *Opt. Express* **7** 56–67
[35] Pallikaris I G and Siganos D S 1994 *J. Refract. Corneal. Surg.* **10** 498–510
[36] Kagan H 2005 *Nucl. Instrum. Methods Phys. Res.* A **541** 221–7
[37] Schein J, Campbell K M, Prasad R R, Binder R and Krishnan M 2002 *Rev. Sci. Instrum.* **73** 18–22
[38] Pan L S, Kania D R, Pianetta P and Landen O L 1990 *Appl. Phys. Lett.* **57** 623–5
[39] Gammel J C and Ballantyne J M 1978 The opfet: a new high speed optical detector *Int. Electron Devices Meeting* vol **24** pp 120–3
[40] Pace E and Sio A D 2010 *Mem. Soc. Astron. Ital.* **14** 84–9
[41] Sugeta T and Mizushima Y 1980 *Japan. J. Appl. Phys.* **19** L27
[42] Campbell J 1985 Chapter 5 phototransistors for light-wave communications *Lightwave Communications TechnologyPhotodetectors (Semiconductors and Semimetals* vol 22*)* ed Tsang W (Amsterdam: Elsevier) part D pp 389–447
[43] Lakshmi B, Chalapati K, Srivastava A K, Arora B M, Subramanian S and Sharma D K 1990 *IEEE Trans. Electron Devices* **37** 1533–5
[44] Romero M A, Martinez M and Herczfeld P R 1996 *IEEE Trans. Microw. Theory Tech.* **44** 2279–87
[45] Jit S and Murty N V N 2006 *Microelectron. J.* **37** 452–8
[46] Sarkar T and Mazumder S K 2007 *Microelectron. J.* **38** 285–98
[47] Chakrabarti P, Jha V, Kalra P and Gupta G 2002 *Microw. Opt. Technol. Lett.* **33** 79–83
[48] Bocharova I A 2003 *J. Appl. Spectrosc.* **70** 948–53
[49] Looi H J, Jackman R B and Foord J S 1998 *Appl. Phys. Lett.* **72** 353–5
[50] Lansley S, Looi H J, Whitfield M and Jackman R 1999 *Diam. Relat. Mater.* **8** 946–51
[51] Maier F, Riedel M, Mantel B, Ristein J and Ley L 2000 *Phys. Rev. Lett.* **85** 3472–5
[52] Ristein J 2006 *J. Phys. D: Appl. Phys.* **39** R71
[53] Shubha R, Pal B B and Khan R U 1998 *IEEE Trans. Electron Devices* **45** 78–84
[54] Alsunaidi M and Al-Absi M 2008 *Opt. Laser Technol.* **40** 711–5
[55] Calvani P, Rossi M C and Conte G 2010 *Opaque-Gate Phototransistors on H-Terminated Diamond* vol 54 (Berlin: Springer) pp 109–12
[56] Shi L, Tang K, Huang J, Zeng Q and Wang L 2010 *Proc. SPIE* **7995** 799526
[57] Wang L, Huang J, Tang K, Zhang J and Xia Y 2011 *Thin-Film Diamond Phototransistors* (Rijeka: InTech) ch 4 (www.intechopen.com/books/optoelectronic-devices-and-properties/thin-film-diamond-phototransistors3)
[58] Element six technologies (www.e6.com/wps/wcm/connect/E6_Content_EN/Home/Materials+and+products/New+materials/)
[59] Conte G, Ricciotti G, Calvani P and Giovine E 2010 *Electron. Lett.* **46** 1614–6
[60] Calvani P, Girolami M, Ricciotti G and Conte G 2011 *Proc. SPIE* **8069** 806908
[61] Conte G, Giovine E, Girolami M, Salvatori S, Bolshakov A, Ralchenko V and Konov V 2012 *Nanotechnology* **23** 075202
[62] See for example Hamamatsu Photonics KK Hamamatsu City J Segmented type si photodiode (www.hamamatsu.com/eu/en/product/alpha/S/4106/index.html#3)
[63] Mazzeo G, Salvatori S, Rossi M C, Scala A D and Conte G 2004 *Optical Position Sensitive Detectors Based on CVD-Diamond Samples* (Singapore: World Scientific) ch 82, pp 515–20
[64] Bergonzo P, Brambilla A, Tromson D, Marshall R, Jany C, Foulon F, Gauthier C, Solé V, Rogalev A and Goulon J 1999 *Diam. Relat. Mater.* **8** 920–6
[65] Salvatori S, Scala A D and Rossi M 2001 *Electron. Lett.* **37** 519–20
[66] See for example Hamamatsu Photonics KK Hamamatsu City J One- and two-dimensional psd (www.hamamatsu.com/us/en/product/alpha/O/4155/index.html; www.hamamatsu.com/jp/en/product/alpha/T/4156/index.html)
[67] Schottky W 1930 *Phys. Z.* **31** 913–25
[68] Wallmark J T 1957 *Proc. IRE* **45** 474–83
[69] Henry J and Livingstone J 2001 *J. Mater. Sci.: Mater. Electron.* **12** 387–93
[70] Koizumi S, Kamo M, Sato Y, Ozaki H and Inuzuka T 1997 *Appl. Phys. Lett.* **71** 1065–7
[71] Pinault-Thaury M A, Tillocher T, Habka N, Kobor D, Jomard F, Chevallier J and Barjon J 2011 *Mater. Sci. Eng.* B **176** 1401–8
[72] Koizumi S, Watanabe K, Hasegawa M and Kanda H 2001 *Science* 292 1899–901
[73] Denisenko A, Aleksov A, Pribil A, Gluche P, Ebert W and Kohn E 2000 *Diam. Relat. Mater.* **9** 1138–42
[74] Cappelluti F, Ghione G, Russell S A O, Moran D A J, Verona C and Limiti E 2015 *Appl. Phys. Lett.* **106** 103504
[75] Ciobanu M *et al* 2016 *Diam. Relat. Mater.* **65** 115–24
[76] Salvatori S, Mazzeo G, Conte G, Rossi M and Ralchenko V 2004 *Diam. Relat. Mater.* **13** 948–53
[77] Salvatori S, Mazzeo G and Conte G 2008 *IEEE Sensors J.* **8** 188–93
[78] Zhou A F 2011 *Opt. Photon. Lett.* **4** 75–81
[79] Franks W A R, Kiik M J and Nathan A 2003 *IEEE Trans. Electron Devices* **50** 352–8
[80] Blouke M M, Cowens M W, Hall J E, Westphal J A and Christensen A B 1980 *Appl. Opt.* 19 3318–21
[81] Holland S E, Groom D E, Palaio N P, Stover R J and Wei M 2003 *IEEE Trans. Electron Devices* **50** 225–38
[82] Bosiers J, Saks N, Michels D, McCarthy D and Peckerar M 1985 Deep-depletion ccds with improved uv sensitivity *Int. Electron Devices Meeting* vol **31** pp 448–51
[83] Li F M and Nathan A 2005 *CCD Image Sensors in Deep-Ultraviolet: Degradation Behaviour and Damage Mechanisms* (*Microtechnology and MEMS*) (Berlin: Springer)
[84] Wei C *et al* 2013 *Nucl. Instrum. Methods Phys. Res.* A **732** 190–4
[85] Rebai M, Cazzaniga C, Croci G, Tardocchi M, Cippo E P, Calvani P, Girolami M, Trucchi D, Grosso G and Gorini G 2015 *J. Instrum.* **10** C03016
[86] Conte G, Girolami M, Salvatori S and Ralchenko V 2007 *Appl. Phys. Lett.* **91** 183515
[87] Girolami M, Allegrini P, Conte G and Salvatori S 2011 *Proc. SPIE* **8073** 807324
[88] Girolami M, Allegrini P, Conte G, Trucchi D M, Ralchenko V G and Salvatori S 2012 *IEEE Electron Device Lett.* **33** 224–6
[89] Girolami M, Conte G, Salvatori S, Allegrini P, Bellucci A, Trucchi D M and Ralchenko V G 2012 *J. Instrum.* **7** C11005
[90] Pacilli M, Allegrini P, Conte G, Spiriti E, Ralchenko V, Komlenok M, Bolshakov A, Khomich A and Konov V 2014 *Nucl. Instrum. Methods Phys. Res.* A **738** 119–25
[91] Kozlov S F and Konorova E A 1971 *Sov. Phys.: Semicond.* **4** 1600–5

[92] Yamada H, Chayahara A, Mokuno Y, Kato Y and Shikata S 2014 *Appl. Phys. Lett.* **104** 102110
[93] Pickles C, Madgwick T, Sussmann R and Wort C 2000 *Diam. Relat. Mater.* **9** 916–20
[94] Rogalin V E, Ashkenazi E E, Popovich A F, Ral'chenko V G, Konov V I, Aranchii S M, Ruzin M V and Uspenskii S A 2012 *Russ. Microelectron.* **41** 464–8
[95] Anoikin E, Muhr A, Bennett A, Twitchen D and de Wit H 2015 Diamond optical components for high-power and high-energy laser applications *Proc. SPIE* **9346** 93460T
[96] Kemp A J, Hopkins J M, Maclean A J, Schulz N, Rattunde M, Wagner J and Burns D 2008 *IEEE J. Quantum Electron.* **44** 125–35
[97] Kaminskii A A, Ralchenko V G and Konov V I 2006 *Laser Phys. Lett.* **3** 171–7
[98] Mildren R P, Sabella A, Kitzler O, Spence D J and McKay A M 2013 *Diamond Raman Laser Design and Performance* (New York: Wiley) pp 239–76
[99] Williams R J, Nold J, Strecker M, Kitzler O, McKay A, Schreiber T and Mildren R P 2015 *Laser Photon. Rev.* **9** 405–11
[100] Ageev V, Bouilov L, Konov V, Kuzmichev A, Pimenov S, Prokhorov A, Ralchenko V, Spitsyn B and Chapliev N 1988 *Sov. Phys.—Dokl.* **33** 840–2
[101] Kononenko T, Ralchenko V, Bolshakov A, Konov V, Allegrini P, Pacilli M, Conte G and Spiriti E 2013 *Appl. Phys.* A **114** 297–300
[102] Forcolin G, Grilj V, Hamilton B, Li L, McGowan M, Murphy S, Oh A, Skukan N, Whitehead D and Zadoroshnyj A 2016 *Diam. Relat. Mater.* **65** 75–82